The Astrophysical Journal Letters, 882:L17 (8pp), 2019 September 10 https://doi.org/10.3847/2041-8213/ab357b

Lunar Xenon and the Origin of the Indigenous Component

K. J. Mathew[1,2] and K. Marti[1]
[1] Department of Chemistry and Biochemistry, University of California San Diego, La Jolla, CA 92093, USA
[2] Actinide Analytical Chemistry, Los Alamos National Lab, MS G740, Los Alamos, NM 87545, USA
Received 2019 June 26; revised 2019 July 23; accepted 2019 July 24; published 2019 September 5

Abstract

Lunar indigenous Xe isotopic abundances provide crucial information on relationships not only between gas reservoirs in the solar protoplanetary disk but also regarding planetary fractionation processes and possible space weather effects due to an active young Sun. The indigenous lunar Xe isotopic composition is not yet firmly established. A verification of previously inferred lunar Xe signatures using rocks of varying compositions from Apollo 16 and 17 missions is made here. Ancient lunar highland rocks carry cosmic-ray-produced spallation and neutron-capture products, fission components due to ^{244}Pu and ^{238}U, as well as terrestrial contamination gas, all complicating the identification of the indigenous lunar Xe component. The present study reveals light and heavy isotopic abundances compatible with terrestrial Xe composition. We conclude that in order to firmly establish indigenous lunar Xe signatures in situ, Xe measurements on the moon in interior samples of anorthositic ejecta from very recent craters should be performed.

Unified Astronomy Thesaurus concepts: Lunar origin (966); Solar abundances (1474); Planetary atmospheres (1244); Isotopic abundances (867)

1. Introduction

The discovery of trapped Xe in Apollo 16 lunar rocks with isotopic abundances that are similar to the terrestrial atmospheric Xe composition (Lightner & Marti 1974) was unexpected, because terrestrial Xe isotopic abundances are vastly different from those in solar-wind-implanted lunar regolith samples, and also from isotopic signatures inferred for protoplanetary disks (Marti & Mathew 2015). Using analyses of selected lunar anorthosites (Bekaert et al. 2017), the presence of atmospheric-like Xe isotopic abundances was recently confirmed. These analyses also indicated the presence of additional Xe components, possibly representing indigenous lunar Xe with slightly lower abundances of the heaviest isotopes in some samples. The possibility of a contamination of lunar material after return was suggested (Niemeyer & Leich 1976), and crushing experiments involving lunar samples demonstrated (Niedermann & Eugster 1992) pickup of some terrestrial Xe. An indigenous lunar origin for a fraction of the trapped component has not been disproved 45 yr later, at the time when a return to the moon is actively being pursued. The observed terrestrial isotopic signature of lunar oxygen strengthens the case for a common evolution of the Earth–Moon system (Pahlevan & Stevenson 2005; Young et al. 2016; Hosono et al. 2019).

The size and geological evolution of planets Mars and Earth are distinct, and similarly fractionated Xe isotopic abundances in their atmospheres are not expected. However, exceptions exist, especially in the abundances of radiogenic ^{129}Xe$_r$ and of fission augmented heavy isotopes (Marti & Mathew 1998; Mathew et al. 1998). The simultaneous occurrence in Martian meteorites of indigenous solar-type Xe and of strongly fractionated atmospheric Xe is well established. The fractionated atmospheric Xe was confirmed by in situ measurements on Mars by the Mars Science Laboratory (Conrad et al. 2016). Further constraints on the early evolution of volatiles in the Martian mantle were provided by the identification of an indigenous reservoir in Chassigny and ALH84001 (Mathew & Marti 2001). After accretion of planet Mars, an early fractionation of volatile I from refractory ^{244}Pu was indicated, which had depleted ^{129}I and its decay product ^{129}Xe$_r$ (Marty & Marti 2002). These authors calculated that radiogenic ^{129}Xe$_r$ and precursor ^{129}I were outgassed from the mantle very early, and that the total amount of Martian ^{129}Xe$_r$ can be estimated to be <1% of the predicted initial ^{129}I abundance. Martian meteorite data also showed that fission Xe$_f$ components due to extinct ^{244}Pu are observed in all nakhlites and in Chassigny (Mathew & Marti 2005; Mathew et al. 2003), in spite of their younger (1.3 Ga) crystallization ages.

A detailed analysis of lunar Xe components in a diverse suite of lunar rocks should not only be useful in further constraining the indigenous lunar Xe composition and early lunar history, but help in planning future work on lunar Xe. The isotopic abundances observed in lunar regolith samples are dominated by implanted solar wind components, and obtaining information on indigenous components is very challenging, as in situ -produced Xe components (galactic and solar cosmic-ray spallation, spontaneous fission of ^{244}Pu/^{238}U as well as neutron-induced fission Xe$_f$ of ^{235}U, and radiogenic ^{129}Xe) are superimposed (Mathew & Marti 2003).

2. Basalts, Anorthosites, and Other Highland Rocks

A large variety of rock types (listed in Table 1) have been included in this work to study lunar Xe isotopic abundances and the indigenous Xe component. All studied samples, except basaltic rock 64455 (Nishiizumi et al. 2009), 70030, and 76010, represent interior chips of crystalline and brecciated rocks. Data of sample 76535, a coarse-grained troctolitic granulite (Lugmair et al. 1976), is included, because data on separated plagioclase serve as a reference for spallation Xe systematics. Rock 72395 is a high-alumina metaclastic rock, while 73215 and 73255 are both light gray breccia, from Station 2 at the base of South Massif (James et al. 1975). Basalts 75035 and 75055 are compositionally distinct from high-Ti, olivine normative basalts, and medium-grained basalt 75075 is from a boulder for which no ^{244}Pu fission Xe$_f$ is

Table 1
Measured Xe Isotopic Abundances in Apollo 16 and 17 Basalts and Breccias

Sample[a]	^{130}Xe 10^{-12} cm^3 g^{-1}	^{130}Xe = 100[b]							
		^{124}Xe	^{126}Xe	^{128}Xe	^{129}Xe	^{131}Xe	^{132}Xe	^{134}Xe	^{136}Xe
Apollo 16 basalts and breccias									
62255,17 (1)[a]	5.83	2.45	2.64	48.04	643.2	520.3	655.5	255.3	216.1
		±0.26	0.22	1.69	11.1	8.8	10	4.2	3.9
60025,83,2[a]	7.01	3.71	4.02	49.3	638.7	516	649.6	252	212.7
		±0.13	0.28	0.86	8.6	6.4	7.8	3.5	3.2
60025,83[a]	9.99	2.57	2.49	47.87	649.5	522.5	660.3	255.8	218.2
		±0.14	0.19	0.88	6.1	4.6	5.4	2.7	2.3
67915,36[b]	1.91	43.19	76.56	128.24	269.9	384.7	230	84.4	76.3
		±1.38	1.93	2.95	7.3	7.7	7.1	4.1	2.4
67915,13[b]	1.65	41.06	70.08	119.61	283	394.3	254.8	89.2	80.5
		±1.92	3.02	5.56	13.2	15.1	11.5	3.9	3.7
67915,34[b]	1.26	41.09	74.15	125.57	284.4	387.5	238.7	91.9	82.3
		±1.45	2.73	3.34	9.7	7.7	10.2	3.9	5.2
62235,25[c]	95.33	45.93	83.94	136.54	187.3	675.2	129.2	37	25.7
		±0.43	0.67	0.77	1	3.2	1.3	0.5	0.5
67015,14[d]	11.13	57.51	97.11	145.5	201.7	365.5	146.5	53.5	50.4
		±1.07	1.82	2.55	4	6.1	3.4	2.3	1.3
67075,8[a]	1.79	10.09	15.79	62.31	560.7	490	578.6	224	188.4
		±0.91	1.58	3.01	18.8	17.1	15.2	7.8	6.8
62295,33[c]	48.91	48.36	86.89	138.75	186.7	585.1	121.9	23.2	13.8
		±0.43	0.57	0.98	1.2	2.8	0.9	0.7	0.3
64455,17[e]	4.96	7.17	10.71	58.56	624.1	502.9	615.3	253.9	221.7
		±0.35	0.32	1.33	8	6.3	7.3	3.2	3.6
67915,67[b]	3.19	42.6	72.8	125.9	267	379	256.7	109.2	98.6
		±2.6	4.4	5.6	30	22	17	4.2	3.8
Apollo 17 basalts and breccias									
70030,2[f]	9.29	61.907	102.02	155.21	210.8	489.9	122.9	20.8	12.7
		±1.157	1.83	2.87	4.8	8.1	2.4	0.7	0.7
75075,66 (2)[g]	9.08	48.327	82.928	133.52	272.1	562	196.6	52.4	37.6
		±0.805	1.265	1.93	3.9	6.5	3	1	0.9
76010,2F[g]	6.08	48.019	81.816	136.02	283.5	413.9	246.2	113.2	110.2
		±1.122	1.434	2.61	4.8	5.7	5.7	3	2.3
73215,260[c]	131.71	52.256	91.534	141.75	181.8	469.3	113.2	20.1	12.3
		±0.324	0.51	0.51	0.7	1.1	0.5	0.2	0.2
76535,64 (3)[h]	34.3	11.545	19.151	64.72	555	502.2	549.3	207.8	175.9
		±0.215	0.319	0.82	3.1	2.9	2.7	1.2	1
76535,66 Pl (3)[h]	12.2	47.131	85.106	130.6	171.2	435.6	116.2	19.5	11.2
		±1.082	1.292	2.56	2.7	3.2	2.2	0.9	0.9
76535,66 Ol (3)[h]	0.39	28.509	41.422	89.33	525.7	561	476.1	183.8	160.1
		±5.689	8.499	15.26	53.8	57.8	40.4	20	15.6
75035,14[g]	7.61	57.88	99.211	151.69	190.3	606.7	109.9	16.4	9.2
		±1.062	1.69	2.14	2.5	5.1	1.7	0.6	0.5
75055,44[g]	6.43	56.46	96.808	149.32	203.1	602.2	120.8	21.5	12.9
		±0.778	1.33	1.68	2	4	1.6	0.5	0.4
72395,18[c]	25.21	52.129	91.485	142.25	187.8	483.3	124.1	31.6	25.9
		±0.675	0.973	1.61	2	2	0.6	0.5	0.4
73255,138[c]	50	56.328	96.916	148.24	202.3	402.1	130.4	32.9	26.2
		±0.558	0.684	1.06	1.2	1.1	0.9	0.4	0.2
78236,1 Pl[i]	50.42	46.17	82.49	130.59	173.01	503.2	116.25	21.14	12.88
		±1.46	1.58	1.73	3.26	7.6	1.14	0.73	0.52
78236,1 Opx[i]	3.41	41.23	67.87	121.51	344.9	520.7	294.23	102.68	84.78
		±1.54	2.38	5.17	36	16.2	8.55	4.81	4.03

Notes.
[a] The samples studied here can be categorized into the following sample types: (a) cataclastic anorthosite, (b) polymict breccia from North Ray crater, (c) melt rock with spinel troctolite, (d) feldspatic fragmental breccia, (e) basaltic melt rock, covered with black glass, (f) highland rock, (g) mare basalt, (h) troctolitic granulite, and (i) norite.
[b] Uncertainties in isotopic ratios represent 95% confidence limits, while those in the ^{130}Xe concentrations are about 12%.
References. (1) Lightner & Marti (1974), (2) Lugmair et al. (1975), (3) Lugmair et al. (1976).

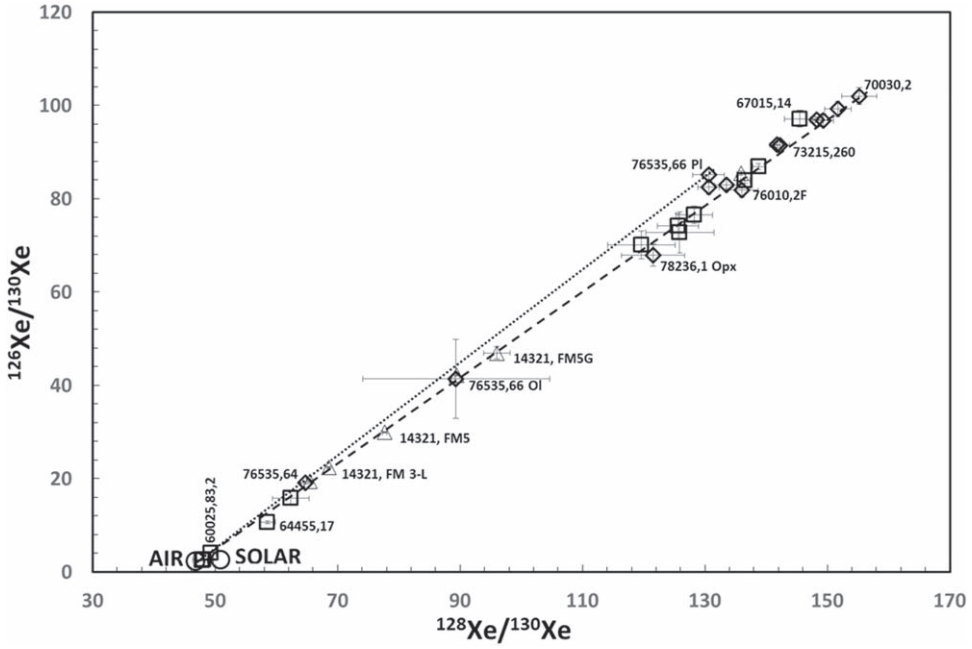

Figure 1. Correlation of light Xe isotope ratios that are affected by spallation Xe component, but not fission Xe.

expected, as the Sm–Nd isochron age is 3.70 ± 0.07 Ga, (Lugmair et al. 1975). Sample 76010 is a single basalt fragment, and is possibly related to crystalline rock 76015, and sample 70030 is a highland rock from Central Cluster. Apollo 16 rocks include 64455, a crystalline highland basalt, and 62295, a spinel troctolite. Studied breccias include 67075, an anorthositic breccia of plutonic origin, 67015 is a light matrix breccia from North Ray crater, and 67915 is a breccia clast. Samples 60025 and 62255 are cataclastic anorthosites; an additional crushed sample of 60025,83 was studied to test for air-Xe contamination in the crushing process. Rock 62295 is a fine-grained spinel troctolite from Buster Crater (Weiblen & Roedder 1973).

Samples of about a quarter of a gram were heated and melted in a double-walled quartz system by radio frequency (RF). Released gases were cleaned in two steps by Ti and Ti–Zr getters, then cryo-separated Xe fractions (Mathew & Marti 2001) were analyzed in the static mode with a magnetic-sector mass spectrometer. Blank measurements were carried out between runs; ^{132}Xe blanks were 1–2 × 10^{-14} cm^3 STP, respectively, in the melt steps. Sensitivity and instrumental mass discrimination were monitored by pipettes of air standards and were found to be constant during the entire set of runs. Tabulated results are corrected for system blank and mass discrimination, and errors include statistical uncertainties in measurements and in blank and background corrections. Uncertainties on isotopic ratios reported represent 95% confidence levels.

3. Data Analyses

Xe isotopic abundances in Apollo 16 and 17 rocks are compiled in Table 1. The Xe concentration in the crushed cataclastic anorthosite 60025,83,2 amounts to 70% of the uncrushed sample and does not indicate Xe uptake in the crushing process. Data for anorthositic breccia 67915 (Marti et al. 1983), troctolite 76535, and basalt 75075 (Lugmair et al. 1975, 1976) are included in the analysis, because of the low trapped Xe concentrations (therefore, these define the spallation and fission Xe end-points for the mineral separates with greater resolution). The data of Fra Mauro rock 14321 with documented ^{244}Pu fission components (Marti et al. 1973) is also included in the correlation plots.

The correlation of fission-shielded isotope ratios ^{126}Xe/^{130}Xe versus ^{128}Xe/^{130}Xe (Figure 1) show a linear trend, revealing two-component mixtures of trapped and in-situ-produced spallation components. Figures 1 and 2 show that lunar trapped Xe isotope ratios are compatible with terrestrial isotopic abundances, except for rock 64455, which plots off the tie-line and indicates solar Xe, not unexpected for an exposed surface of low ablation (Nishiizumi et al. 2009). As Figures 1 and 2 show, spallation Xe ratios are not uniform, but define a range based on variable compositions of the Ba/rare earth element (REE) ratios, and variable cosmic-ray shielded locations, as indicated by ^{130}Ba neutron-capture excesses $^{131}Xe_n$ (see Table 1; only the spallation component from Ba is characterized using cross-section measurements at representative cosmic-ray energies, see Mathew et al. 1994, 1989). A better approximation to observed spallation component is the actual spectra observed in different rock types with varying contributions from Ba and REE and estimated from correlation plots}. In the figures the spallation sector is limited by 12021 data (Marti & Lugmair 1971), 14160-8 (Marti et al. 1973), and by 76535 plagioclase data. For the analyses of fission components we adopt the terrestrial Xe signature, as previously inferred in 14321 and in anorthosites (Marti et al. 1973; Lightner & Marti 1974; Bekaert et al. 2017). Other correlation plots support a terrestrial Xe composition within error limits, except for large observed neutron-capture excesses $^{131}Xe_n$. No neutron-capture excesses $^{128}Xe_n$ are observed, reflecting low lunar ^{127}I abundances.

Surviving radiogenic components from ^{129}I show up as $^{129}Xe_r$ excesses in Figure 3, while in-situ-produced fission components are visible as excesses on the heavy isotopes in Figures 4(a) and (b); these data include fission components

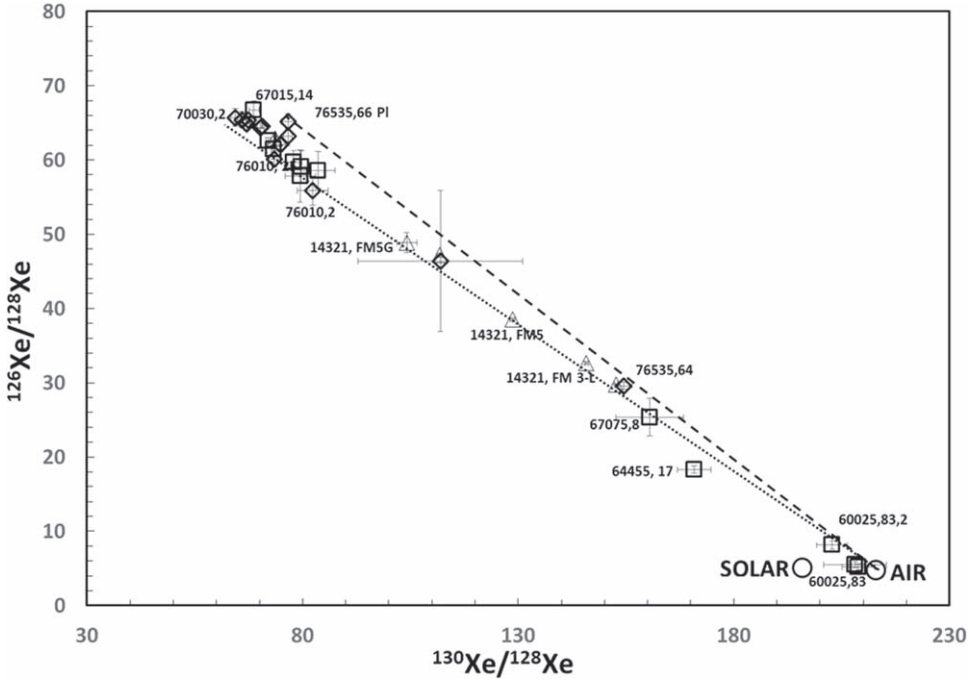

Figure 2. Correlation of light Xe isotope ratios that are affected by spallation Xe component, but not fission Xe.

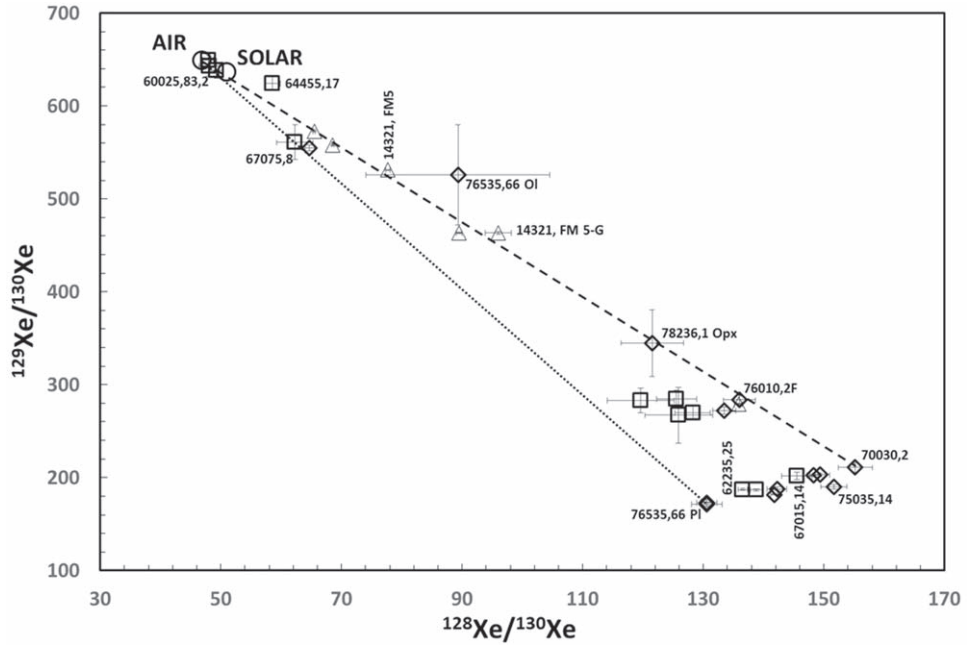

Figure 3. Correlation of Xe isotope ratios that are affected by the spallation component and radiogenic Xe from decay of extinct ^{129}I.

from neutron capture in ^{235}U. The fission component(s) can be evaluated using known fission yield ratios and calculated excesses on ^{136}Xe, ^{134}Xe, and ^{132}Xe (Table 2). Excesses would deviate from those expected for fission components, if heavy Xe isotope abundances differ from adopted terrestrial values (Bekaert et al. 2017). For the correction of spallation components in measured data, we use interpolated spallation spectra, based on composition and shielding data of fission-shielded isotopes. The used reference spallation spectrum (Table 2) matches the spectrum under investigation, when zero values are obtained after subtraction of trapped + spallation components at fission-free isotopes, while total fission components are revealed as excesses on the heavy isotopes. We checked this approach in additional analyses (ratios ^{126}Xe/^{128}Xe versus ^{130}Xe/^{128}Xe) and heavy isotopes show either zero excesses or fission components.

The identification of the ^{244}Pu fission component in ancient terrestrial zircons made use of all fission excesses, including ^{131}Xe$_f$ (Turner et al. 2007), but the latter isotope cannot be used in lunar fission components, because neutron-capture-produced ^{131}Xe$_n$ components are prohibitive. Surface-correlated components, including neutron-induced fission Xe$_{nf}$, were extensively studied in lunar rock 14301 (Bernatowicz et al. 1980). The fission-excess ratios ^{134}Xe/^{136}Xe versus ^{132}Xe/^{136}Xe in

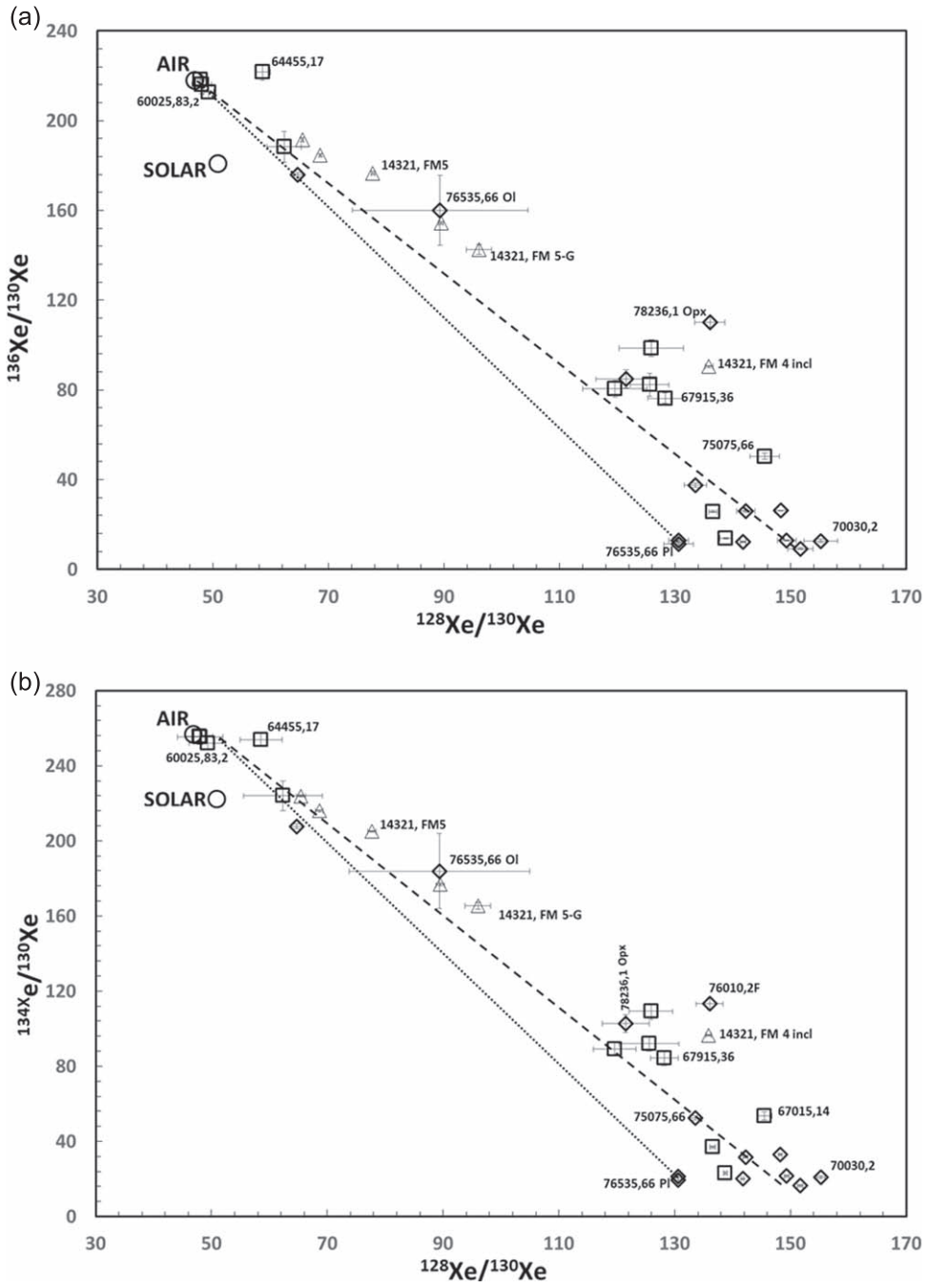

Figure 4. (a) Correlation of Xe isotope ratios that are affected by fission components. (b) Correlation of Xe isotope ratios that are affected by fission components.

Figure 5 is useful to disentangle components due to $^{244}Pu_f$, $^{238}U_f$, and $^{235}U_{nf}$ separately for Apollo 16 and 17 rocks (the 14321 data are also plotted for reference).

Although the inferred $^{244}Pu_f$ and $^{238}U_f$ fission components cannot strictly be used to determine fission retention (closing) times, as they may be affected by inherited components, the calculated fission $^{136}Xe_f$ and spallation $^{126}Xe_c$ concentrations are given in Table 2. These data are useful in cases where elemental abundances are known.

The concentration $^{136}Xe_f$ from ^{238}U is calculated using Equation (1)

$$^{136}Xe_f[^{238}U] = [^{238}U]\ \lambda_{sf}/\lambda_{238}\ Y_{136}(e^{\lambda t} - 1) \quad (1)$$

where λs are the decay constants, Y is the fission yield of ^{136}Xe, and $[^{238}U]$ is the ^{238}U content of the material. The concentration of fission Xe from ^{244}Pu is calculated using Equation (2)

$$^{136}Xe_f[^{244}Pu] = [^{244}Pu]\ \lambda_{sf}/\lambda_{244}\ Y_{136} \quad (2)$$

where λs are the decay constants, Y is the fission yield of ^{136}Xe, and $[^{244}Pu]$ is the ^{244}Pu content of the material. The expected ratios of fission components at time t are calculated from initial $^{244}Pu/^{238}U$ ratios.

For 14321 samples from Fra Mauro crater a $^{244}Pu/^{238}U$ ratio of 1.3×10^{-4} was obtained and an age 3.95 Ga was inferred (Marti et al. 1973). An U–Pb age of 3943 ± 5 Ma was reported for apatite and merrilite grains from breccia 14321 (Snape et al. 2016),

Table 2
Fission Xe Concentrations and Spectra

Sample	Ref. Spectra[a]	$^{126}Xe_C$	$^{136}Xe_F$	$^{132}Xe/^{136}Xe$	$^{134}Xe/^{136}Xe$
67015,14	12021 (50%) + 76535 (50%)	10.6	5.6 ± 0.6	0.88 ± 0.04	0.91 ± 0.02
67915,67	12021	2.3	1.3 ± 0.2	0.75 ± 0.10	0.88 ± 0.04
67915,34	12021	0.9	0.4 ± 0.1	0.54 ± 0.16	0.82 ± 0.07
67915,36	12021	1.4	0.6 ± 0.2	0.58 ± 0.12	0.80 ± 0.07
67915,13	12021	1.1	0.3 ± 0.1	0.46 ± 0.14	0.68 ± 0.10
62235,25	76535 Plag.	77.9	9.9 ± 1.3	0.52 ± 0.06	0.83 ± 0.04
62295,33	76535 Plag.	41.4	1.6 ± 0.4	0.54 ± 0.16	0.83 ± 0.08
67075,8	76535 Plag.	0.24	0.1 ± 0.1	0.62 ± 0.16	0.84 ± 0.10
64455,17	12021	0.42	1.9 ± 0.2	0.59 ± 0.12	0.83 ± 0.06
60025,83	12021	0.08	<0.2		
62255,17	12021	0.03	<0.2		
70030,2	14160	9.3	0.3 ± 0.2	0.79 ± 0.11	0.91 ± 0.07
75075,66	12021	7.3	0.1 ± 0.2	0.74 ± 0.14	0.93 ± 0.04
76010,2F	12021	4.8	4.3 ± 0.4	0.73 ± 0.04	0.87 ± 0.02
73215, 260	12021 (50%) + 76535 (50%)	117.7	6.0 ± 2.3	0.85 ± 0.07	0.94 ± 0.02
76535,64	14160	5.8	0.1 ± 0.3	0.90 ± 0.16	0.92 ± 0.04
76535,66 Plag.	76535 Plag.	10.1	<0.1		
76535,66 Oliv.	76535 Plag.	0.15	0.1 ± 0.1	0.92 ± 0.2	0.93 ± 0.09
75035,14	12021	7.4	0.4 ± 0.1	0.66 ± 0.16	0.90 ± 0.07
75055,44	12021	6.1	0.6 ± 0.1	0.61 ± 0.14	0.90 ± 0.04
72395,18	14160,8	22.5	4.9 ± 1.5	0.59 ± 0.07	0.88 ± 0.05
73255, 138	14160,8	47.4	9.6 ± 1.3	0.85 ± 0.04	0.92 ± 0.02
78236,1 Plag.	12021	40.5	0.7 ± 0.2	0.68 ± 0.14	0.90 ± 0.07
78236,1 Opx.	12021 (40%) + 76535 (60%)	2.24	0.5 ± 0.2	0.87 ± 0.10	0.93 ± 0.05
FM 1+2	14160,8	16.1	5.8 ± 0.7	0.79 ± 0.03	0.90 ± 0.02
FM3 "light"	14160,8	16.6	5.0 ± 0.5	0.81 ± 0.04	0.89 ± 0.02
FM3 "dark"	14160,8	30.6	12.8 ± 1.0	0.82 ± 0.02	0.88 ± 0.02
FM4 bas. incl.	14160,8	32.5	25.0 ± 1.1	0.88 ± 0.02	0.91 ± 0.02
FM5	14160,8	24.1	10.1 ± 0.6	0.80 ± 0.02	0.87 ± 0.02
FM5G	14160,8	11.4	4.5 ± 0.6	0.82 ± 0.03	0.86 ± 0.02

Note.
[a] Selected to provide best fit to fission-shielded (light) isotopes; concentrations are in units of 10^{-12} cm^3 STP g^{-1}. The uncertainties in $^{136}Xe_F$ (units of 10^{-12} cm^3 STP g^{-1}) and in the fission spectra are linear additions of isotopic uncertainties in data (95% confidence limits) plus those in selected reference spectra.$^{136}Xe_U$ are estimates of ^{238}U-supported fission concentrations (units of 10^{-12} cm^3 STP g^{-1}) for ages of 3.95 Ga. Measured ratios $^{132}Xe/^{136}Xe$ and $^{134}Xe/^{136}Xe$ for ^{244}Pu and for [^{238}U] are 0.876 ± 0.031 [0.578 ± 0.013], and 0.921 ± 0.027 [0.827 ± 0.008], respectively (Alexander et al. 1971).

while a $^{207}Pb/^{206}Pb$ age of 3936 ± 8 Ma was obtained for a granular zircon grain, interpreted as an impact date and marking the final extrusion of KREEP (basaltic rocks characterized by high K, REE, and P contents) magma (Thiessen et al. 2019). A larger ratio of 3.2×10^{-4} was reported for a troctolitic anorthosite inclusion in breccia 67915 (Marti et al. 1983), corresponding to an age of 4.3 Ga, assuming in situ production of the fission components.

4. Discussion and Conclusions

Figure 1 shows that two-component mixtures of trapped and spallation Xe, with limiting spectra from rocks 12021 and 76535 Plag (plagioclase), can account for observed light Xe isotopic abundances. Figure 1 further reveals that Xe in rock 64455 is not consistent with a terrestrial trapped Xe composition, and Figure 2 confirms this conclusion. The 64455 data plot off the limiting correlation line, suggesting the presence of implanted solar Xe, consistent with spallation added to solar Xe (Meshik et al. 2014). Nishiizumi et al. (2009) documented that 64455 experienced an irradiation on the lunar surface, and the identification of a solar Xe component is consistent with this scenario. Uncertainties in the data do not rule out an additional minor component with terrestrial abundances, like those observed in anorthositic breccia (e.g., 67915) that contain very small trapped components (Table 1).

Figure 3 shows that among Apollo 16 anorthositic breccia there is no clear case exhibiting radiogenic $^{129}Xe_r$ excesses, while $^{129}Xe_r$ excesses are observed in many basalts and in olivine of troctolite 76535, but not in pyroxene, which also indicates no fission excess. Figures 4(a) and (b) reveal fission excesses separately in heavy Xe isotopes of Apollo 16 and 17 rocks, and relative excesses that are comparable to those in Fra Mauro rock 14321. The latter fission data were reported to include ^{244}Pu components in addition to ^{238}U spontaneous fission (Marti et al. 1973). Figure 5 confirms the presence of ^{244}Pu fission components, and it also shows that excesses can be split into components due to $^{244}Pu_f$, $^{238}U_{sf}$, and $^{235}U_{nf}$. The latter appears as possible minor additions only in some Apollo 17 rocks. None of the data plot outside the three-component fission range, a hint that could indicate an error in adopting terrestrial isotopic abundances.

As discussed earlier, in case of Mars the in situ study (Conrad et al. 2016) of the Martian atmospheric Xe composition, confirmed previously reported isotopic abundances obtained in Martian meteorites. Therefore, a study on the moon of lunar Xe isotopic abundances should clarify the composition of indigenous Xe, but the issue of how to locate indigenous Xe still remains. An interior sample is not shielded from cosmic-ray bombardment and small spallation components (Table 2) are only found in ejecta from recent craters. For a study of indigenous Xe isotopic data, a

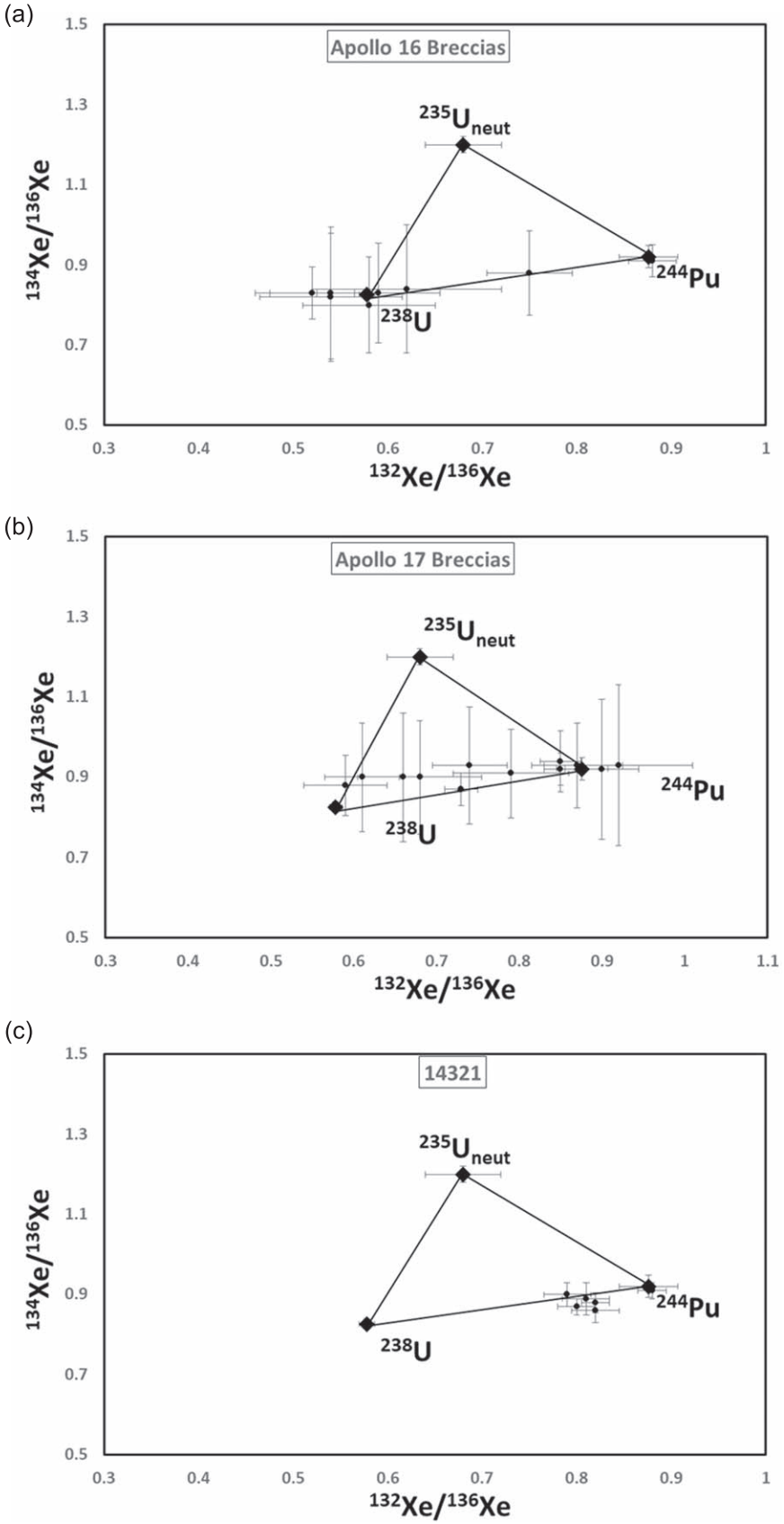

Figure 5. Calculated excess fission Xe ratios from Table 2 are shown, revealing the relative contribution of the three inferred fission components (^{244}Pu, ^{238}U, and $^{235}U_{neut}$).

low abundance of $^{244}Pu_f$ and $^{238}U_f$ fission components will be advantageous, as shown in this work. The heavy Xe isotopes are critical in resolving fractionation associated with processes that created the indigenous components.

Martian atmospheric Xe was characterized as fractionated solar Xe (Mathew et al. 1998; Conrad et al. 2016), which represents the indigenous component observed in Martian meteorites (Mathew & Marti 2001). Although inferred fractionations in terrestrial and Martian atmospheric Xe are similar, the relative abundances in the heavy isotopes differ in detail. If similar fractionation mechanisms were involved in deriving the two planetary atmospheres, the reservoirs of the two components must differ, and they possibly may represent different sources in the protoplanetary disk (Marti & Mathew 2015). It was also noted by these authors that heavy Xe isotopic abundances are strongly affected by a Xe-HL component (Xe component in nano-diamonds of pre-solar origin and enriched in both heavy and light isotopes), and that differences between the atmospheres of Earth and Mars are consistent with varying contributions from Xe-HL.

The results of this lunar rock study confirm that trapped lunar Xe is consistent with present terrestrial Xe isotopic abundances. However, evidence was reported that terrestrial atmospheric Xe may have evolved (Avice et al. 2018), and that the early lunar surface may have been affected by space weather due to the young Sun (Saxena et al. 2019), further complicating the question of origin. On the other hand, Xe components of non-atmospheric composition were reported in terrestrial reservoirs (Caffee et al. 1999; Lee et al. 2009; Holland et al. 2009). Non-terrestrial signatures, as observed in old terrestrial environments, were explained by meteoritic influx (Schoenberg et al. 2002; Gourier et al. 2019), or may reveal residual primitive components incorporated together with modern atmospheric components, as was observed in Martian meteorites (Mathew et al. 1998). In summary, this study shows that in situ measurements on the moon should help to clarify isotopic abundances of indigenous Xe. An interior sample of ejecta from a recent crater is required, and boulders with low U, ^{244}Pu, Ba, and REE abundances, like anorthosites, would be suitable for such study.

Constructive comments from an anonymous reviewer are greatly appreciated. LSAPT and the lunar sample curators are thanked for allocating samples used for this research. Discussions with numerous colleagues and the assistance in the laboratory by C. Black and K.R. Goldman are acknowledged. Research was supported by NASA grants NAG5-8167, NAG5-12983 and NNG 05GJ08G to K. Marti. This publication has been assigned LA-UR-19-25932.

ORCID iDs

K. J. Mathew https://orcid.org/0000-0002-1794-4476
K. Marti https://orcid.org/0000-0002-5054-0510

References

Alexander, E. C., Jr., Lewis, R. S., Reynolds, J. H., & Michel, M. C. 1971, Sci, 172, 837
Avice, G., Marty, B., Burgess, R., et al. 2018, GeCoA, 232, 82
Bekaert, D. V., Avice, G., Marty, B., Henderson, B., & Gudipati, M. S. 2017, GeCoA, 218, 114
Bernatowicz, R. J., Hohenberg, C. M., Hudson, G. B., et al. 1980, LPSC, 11, 629
Caffee, M. W., Hudson, G. B., Velsko, C., et al. 1999, Sci, 285, 2115
Conrad, P. G., Malespin, C. A., Franz, H. B., et al. 2016, E&PSL, 454, 1
Gourier, D., Binet, L., Calligaro, T., et al. 2019, GeCoA, 258, 207
Holland, G., Cassidy, M., & Ballentine, C. J. 2009, Sci, 326, 1522
Hosono, N., Karato, S. I., Makino, J., & Saitoh, T. R. 2019, NatGe, 12, 418
James, O. B., Brecher, A., Blanchard, D. P., et al. 1975, LPSC, 6, 547
Lee, J. Y., Marti, K., & Wacker, J. F. 2009, JGRE, 114, 4003
Lightner, B. D., & Marti, K. 1974, LPSC, 5, 2023
Lugmair, G. W., Marti, K., Kurtz, J. P., & Scheinin, N. B. 1976, LPSC, 7, 2009
Lugmair, G. W., Scheinin, N. B., & Marti, K. 1975, LPSC, 6, 1419
Marti, K., Aeschlimann, U., Eberhardt, P., et al. 1983, LPSC, 14, 165
Marti, K., Lightner, B. D., & Lugmair, G. W. 1973, Moon, 8, 241
Marti, K., & Lugmair, G. W. 1971, LPSC, 2, 1591
Marti, K., & Mathew, K. J. 1998, InEPS, 107, 425
Marti, K., & Mathew, K. J. 2015, ApJL, 806, L30
Marty, B., & Marti, K. 2002, E&PSL, 196, 251
Mathew, K. J., Kim, J. S., & Marti, K. 1998, M&PS, 33, 655
Mathew, K. J., & Marti, K. 2001, JGR, 106, 1401
Mathew, K. J., & Marti, K. 2003, M&PS, 38, 627
Mathew, K. J., & Marti, K. 2005, JGRE, 110, E12S05
Mathew, K. J., Marty, B., Marti, K., & Zimmermann, L. 2003, E&PSL, 214, 27
Mathew, K. J., Rao, M. N., Michel, R., & Prescher, K. 1989, Metic, 24, 300
Mathew, K. J., Rao, M. N., Weber, H. W., Herpers, U., & Michel, R. 1994, NIMB, 94, 449
Meshik, A., Hohenberg, C., Pravdivtseva, O., & Burnett, D. 2014, GeCoA, 127, 326
Niedermann, S., & Eugster, O. 1992, GeCoA, 56, 493
Niemeyer, S., & Leich, D. A. 1976, LPSC, 7, 587
Nishiizumi, K., Arnold, J. R., Kohl, C. P., et al. 2009, GeCoA, 73, 2163
Pahlevan, K., & Stevenson, D. J. 2005, E&PSL, 262, 438
Saxena, P., Killen, R. M., Airapetian, V., et al. 2019, ApJL, 876, L16
Schoenberg, R., Kamber, B. S., Collerson, K. D., & Moorbath, S. 2002, Natur, 418, 403
Snape, J. F., Nemchin, A. A., Grange, M. L., et al. 2016, GeCoA, 174, 13
Thiessen, F., Nemchin, A. A., Snape, J. F., & Whitehouse, M. J. 2019, M&PS, 54, 1720
Turner, G., Busfield, A., Crowther, S. A., et al. 2007, E&PSL, 261, 491
Weiblen, P. W., & Roedder, E. 1973, LPSC, 4, 681
Young, E. D., Kohl, I. E., Warren, P. H., et al. 2016, Sci, 351, 493